Advanced Characterization of Nanoporous Gold

A.A. El-Zoka[*], R.C. Newman[*], B. Langelier[**], and G. Botton[**]

[*]Department of Chemical Engineering and Applied Chemistry, University of Toronto
Room WB254, 200 College St., Toronto, ON, Canada, ayman.elzoka@mail.utoronto.ca.
[**]Department of Materials Science and Engineering and Canadian Centre for Electron Microscopy, McMaster University, Hamilton, ON, Canada.

Abstract

The interest in nanoporous metals, formed by controlled dealloying of noble metal alloys, has been increasing due to the promising capabilities of such materials. The functionality of nanoporous gold (NPG) is heavily affected by attributes such as ligament size, and local and global chemical composition [1][2]. Realizing the full potential behind NPG as a functional material can only be facilitated by the analysis of the porous structure at its natural length scale – that is, the nanometre scale [3]. Atom Probe Tomography (APT) on NPG is demonstrated, obtaining structural and chemical properties of NPG at near-atomic resolution.

Keywords: dealloying; nanoporous metals; atom probe tomography; characterization

1 Introduction

Atom Probe Tomography (APT) is capable of providing 3D analysis of many materials at the nanometer, and even sub-nanometre scale. Due to the high porosity, APT on NPG was deemed as difficult. Pores are highly likely to result in mechanical failure of the sample during analysis [4][5]. The Cu-filling electrochemical method presented here overcomes such complications and is applicable, in principal, to a wide range of pore sizes and solutions.

2 Experimental Procedure

A sample with the nominal surface area of ~0.2 cm^2 was cut out of a cold-rolled 200 µm sheet of $Ag_{77}Au_{23}$ (at. %). The sample was annealed at 925 °C for 15 h in H_2–Ar atmosphere. The sample was dealloyed potentiostatically in a solution of 0.5 M $HClO_4$ at a potential of 550 mV vs. MSE (Mercury/Mercurous Sulfate Electrode/sat. K_2SO_4), until the removal of 5 C/cm^2 .

To provide structural support to the porous layer, elimination of porosity was achieved through inner-pore electrodeposition of Cu. For filling the pores, Cu is electrodeposited through the following steps. Immediately following removal from the de-ionized water, samples were placed into a solution of 50 mM $CuSO_4$ + 0.1 M H_2SO_4. The deposition was carried out at room temperature. To identify the range of potentials in which Cu deposits on to the porous layer, a cyclic voltammogram ranging from 0 V to -0.4 V at a slow scan rate (0.1 mV/s), shown in figure 1, was obtained.

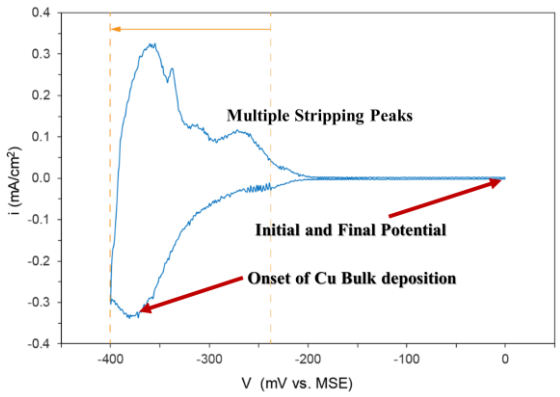

Figure 1: Cyclic voltammogram of dealloyed NPG at a scan rate of 0.1 mV/s in 50 mM $CuSO_4$ + 0.1 M H_2SO_4.

In the same solution, stepped potentiostatic UPD of Cu at progressively more negative potentials was performed until the final stage of bulk deposition (at -0.4 V). For all of the potentiostatic steps (except the final one), progressing to more negative potential was not done until the current density decayed to zero. The charge deposited at each step is shown in Table 1. All electrochemical experiments were performed using a Gamry Reference 600™ potentiostat. The distributed nature of the UPD with potential is typical for dealloyed material.

Deposition Voltage (mV)	Charge Deposited per Nominal Surface Area (mC/cm^2)
-240	2.40
-300	14.1
-323	12.7
-348	22.8
-370	27.4
-400	3484

Table 1: Potentials of deposition with the charge deposited at each step.

Specimens for APT were prepared using a Zeiss NVision 40 dual-beam focused ion beam (FIB), and scanning electron microscope (SEM). APT analysis was conducted using a Cameca local electrode atom probe (LEAP) 4000X HR. Experiments were conducted under high vacuum at an approximate specimen temperature of 59 K.

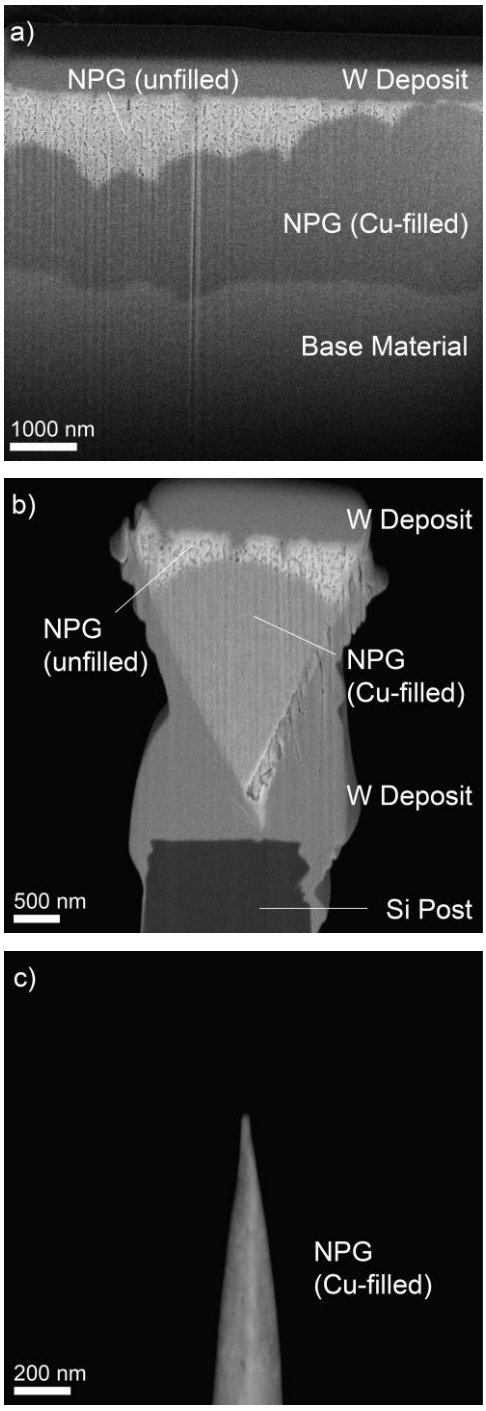

Figure 2: SEM images of a) material cross-section showing the dealloyed layer after deposition of Cu, b) FIB liftout wedge attached to Si post, c) APT sample after FIB sharpening.

Field evaporation was promoted by holding the specimen at a DC voltage in the range of < 6 kV and illuminating the tip with a UV laser (λ = 355 nm) at a pulse rate of 100-125 kHz and a pulse energy of 50 pJ. The rate of evaporation was controlled by varying the DC voltage, and set to a target value of 0.005 ions/pulse (0.5 %).

3 Results and Discussion

Cross-sections of the dealloyed and Cu-filled material, such as shown in figure 2a, are examined to reveal the depth of the dealloying (i.e. the thickness of the nanoporous layer) and the degree of Cu filling. As seen in figure 2a, the dealloyed layer extends to a fairly uniform depth of approximately 2.8 μm below the sample surface. That same image also shows regions of the nanoporous layer to be not completely filled by the Cu. There are small unfilled regions (seen in figure 2a,b) of the layer, mostly found adjacent to the sample surface. The deepest portions of the dealloyed layer are all filled. This partial filling can be attributed to a deficient concentration of Cu ions in the solution, leading to Cu deposition on the surface before filling the entire porous layer. Increasing this concentration (to the extent of 0.5 M – 1M) yields a more completely filled dealloyed layer.

Atomic scale chemical mapping of the porous structure was achieved (figures 3-5). Due to the efficiency of the Cu filling, a larger volume of NPG-Cu was analyzed by APT, compared to that presented in Pfeiffer's work [5]. Atom maps of Cu-filled NPG are shown in figure 3. The results show that the Cu-rich region, representing the filling, and the Ag/Au-rich region, representing the NPG, form complementary networks in the 3D data. Also, the atom maps reveal pores as small as 10 nm.

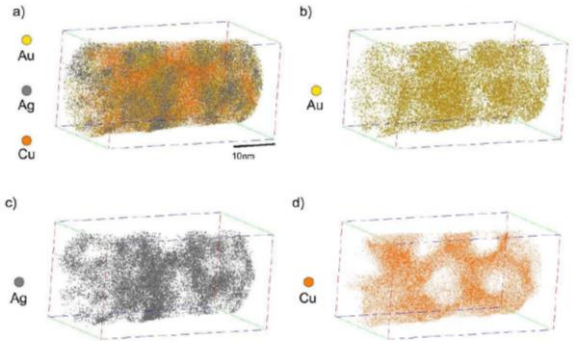

Figure 3: a) 3D APT atom map of NPG, showing Au, Ag, and Cu atoms, and individual element maps for b) Au, c) Ag, d) Cu atoms.

A composition profile generated across a single ligament from the cross-section in figure 4 is shown in figure 4b. In agreement with the theoretical models for ligament structure, the gold content decreases from high levels at the surface to reach its minimum at the core and vice versa for Ag. The ligament composition at the core is close to the composition of the precursor (77 at. % Ag, 23

at. % Au), supporting further the formation mechanism widely accepted, as a competition between dissolution of Ag and Au surface diffusion [3].

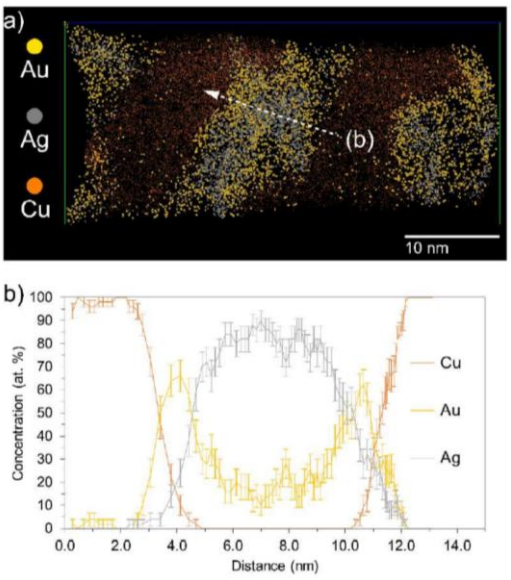

Figure 4: a) APT atom map of a 2 nm cross-section from a reconstructed volume, showing Au, Ag, Cu atoms. b) 1D concentration profile through a ligament, as indicated on (a).

Figure 5 shows the result of mapping the compositions of all elements across a 2 nm thick cross-section, taken longitudinally from a reconstructed volume. Here, the composition variation between Ag and Au in the ligaments can be observed in directions both normal and parallel to the specimen axis.

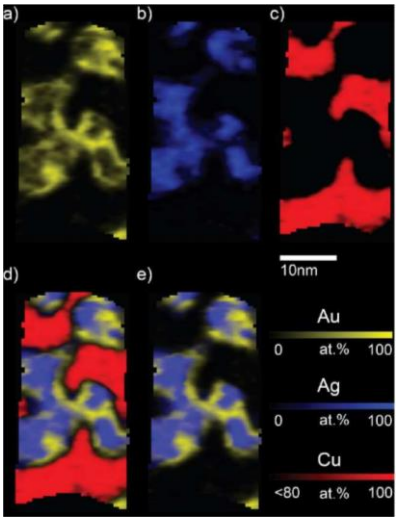

Figure 5: Longitudinal 2 nm cross-section of a reconstructed volume showing concentrations of a) Au (yellow), b) Ag (blue), c) Cu (red), along with d,e) composite images.

This is the first demonstration, at such a fine length scale, that the ligament cores can be literally original alloy. Most dealloying studies either use nitric acid (which gives coarser ligaments), or longer electrochemical exposures, both of which allow depletion of Ag from the ligaments during coarsening. The presence of ion trajectory aberrations affecting the data (evidenced again by the apparent intermixing of the ligament with the Cu at the edges) suggests the composition values at the interface should only be considered semi-quantitatively.

4 Future Work

To extend and clarify the analysis presented above, APT on NPG made by dealloying of ternary alloy precursors ($Ag_{77}Au_{22}Pt_1$ and $Ag_{77}Au_{20}Pt_3$) will be investigated. Such porous materials have finer ligament and pore sizes [6]. In an effort to understand the refining effect of Pt and the mechanism involved, APT data will also be correlated with STEM tomography. In addition to chemical profiling of individual ligaments, chemical composition across the dealloying interface and the extent of Pt redistribution in the dealloyed layer will be investigated.

5 Conclusions

The challenge of analyzing nanoporous materials by APT has been overcome in this work through development of a reproducible process for complete pore filling. Thus, atomic scale characterization of NPG was facilitated. Core-shell structure of the nanoligaments formed in the dealloyed structure was revealed through several cross-sectional and chemical analyses.

6 Acknowledgments

The authors acknowledge support by an NSERC Discovery Grant and Accelerator Supplement awarded to R.C Newman. The authors acknowledge the facilities, scientific and technical assistance from the Canadian Centre for Electron Microscopy (CCEM) a facility supported by the Canada Foundation for Innovation under the Major Science Initiative program, NSERC and at McMaster University (also supported by NSERC and other government agencies).

References

[1] M. Yan, T. Jin, Q. Chen, H. E. Ho, T. Fujita, L. Y. Chen, M. Bao, M. W. Chen, N. Asao, and Y. Yamamoto, “Unsupported nanoporous gold catalyst for highly selective hydrogenation of quinolines,” Org. Lett. 15, (2013): pp. 1484–1487.

[2] L. V Moskaleva, S. Röhe, A. Wittstock, V. Zielasek, T. Klüner, K. M. Neyman, and M. Bäumer, “Silver residues as a possible key to a remarkable oxidative catalytic activity of nanoporous gold,” Phys. Chem. Chem. Phys. 13, (2011): pp. 4529–4539.

[3] T. Fujita, P. Guan, K. McKenna, X. Lang, A. Hirata, L. Zhang, T. Tokunaga, S. Arai, Y. Yamamoto, N. Tanaka, Y. Ishikawa, N. Asao, Y. Yamamoto, J. Erlebacher, and M. Chen, “Atomic origins of the high catalytic activity of nanoporous gold,” Nature Materials 11, (2012): pp. 775–780.

[4] J. Weber, J. Barthel, F. Brandt, M. Klinkenberg, U. Breuer, M. Kruth, and D. Bosbach, “Nano-structural features of barite crystals observed by electron microscopy and atom probe tomography,” Chem. Geol. 424, (2016): pp. 51–59.

[5] B. Pfeiffer, T. Erichsen, E. Epler, C. A. Volkert, P. Trompenaars, and C. Nowak, “Characterization of nanoporous materials with atom probe tomography,” Microscopy and Microanalysis 21, (2015): pp. 557-563.

[6] A.A. Vega, and R. C. Newman, “Nanoporous metals fabricated through electrochemical dealloying of Ag-Au-Pt with systematic variation of Au:Pt ratio,” Journal of the Electrochemical Society 161, (2014): pp. C1-C10.

[7] J. Erlebacher, and R. Seshadri, “Hard Materials with Tunable Porosity,” MRS Bull., vol. 34, pp. 561–568, 2009.